

Edge emission from 265 nm UV-C LEDs grown by MBE on bulk AlN

Shivali Agrawal,^{1, a)} Hsin-Wei S. Huang,^{2, b)} Debaditya Bhattacharya,² Madhav Ramesh,² Krzesimir Szkudlarek,³ Henryk Turski,^{2,3} Vladimir Protasenko,² Huili Grace Xing,^{2,4,5} and Debdeep Jena^{2,4,5, c)}

¹⁾Department of Chemical and Biomolecular Engineering, Cornell University, Ithaca, USA

²⁾Department of Electrical and Computer Engineering, Cornell University, Ithaca, USA

³⁾Institute of High Pressure Physics PAS (Unipress), Warsaw, Poland

⁴⁾Department of Materials Science and Engineering, Cornell University, Ithaca, USA

⁵⁾Kavli Institute at Cornell for Nanoscale Science, Cornell University, Ithaca, USA

UV-C LEDs pseudomorphically grown by MBE on bulk AlN substrates emitting at 265 nm are demonstrated. High current density up to 800 A/cm², 5 orders of on/off ratio, and low differential on-resistance of 2.6 mΩ·cm² at the highest current density is achieved. The LED heterostructure has a high refractive index waveguide core surrounded by n- and p-cladding layers similar to a laser diode designed for mode confinement at 270 nm to facilitate edge emission and collection of photons. Edge-emitting devices are made by cleaving the fabricated LEDs along the *m*-plane of the wurtzite crystal. Electrical injection results in emission of high energy 4.7 eV photons that are collected from the cleaved edge of the LEDs corresponding to the optical bandgap of the AlGaN active region. The contribution of power dissipation across the n- and p-regions of the diode is discussed. The n-contact resistance to n-AlGaN is identified as the largest contributor to the series resistance of the LED in the present generation of devices.

High Al composition AlGaN-based UV-C (200 nm < $\lambda_{\text{emission}}$ < 280 nm) light emitting diodes (LEDs) and laser diodes (LDs) on bulk AlN substrates are attractive for the development of deep ultraviolet light sources. These diodes have applications in sterilization, disinfection, lithography, and machining.¹ However these LEDs currently face challenges with their low external quantum efficiency, short lifetimes and rapid degradation at high injection.^{1,2} Investigation of these structures using different growth techniques can provide valuable insights into solving the current challenges. Metal-organic chemical vapor deposition (MOCVD) and molecular beam epitaxy (MBE) remain the most common growth techniques for the development of these diodes. Recently reported UV-C laser diodes grown by MOCVD on bulk AlN substrates have shown impressive performance³ but are still plagued by short lifetimes.²

While MOCVD is a scalable and commercially relevant growth technique, MBE offers ultra-high vacuum environment and hydrogen-free growth with ultrapure elemental sources which result in films with low C, H, Si, and O impurities as seen by time-of-flight secondary ion mass spectrometry (SIMS) measurements.⁴ Additionally, lower growth temperatures in MBE result in reduced passivating defects that tend to form in high temperature epitaxy.⁵

The crystal quality of the underlying AlN is important for device performance.⁶ AlGaN films grown on bulk AlN substrates with low threading dislocation density (TDD) increase the internal quantum efficiency (IQE), carrier injection efficiency (CIE), and lifetime of devices.^{7–10} An earlier study has demonstrated the first MBE grown optically-pumped 280 nm AlGaN-based laser on a bulk AlN substrate,¹¹ highlighting

the optical quality of AlGaN thin films grown by MBE. We also recently demonstrated the first MBE grown high Al content AlGaN p-n junction diodes appropriate for electrical injection on bulk AlN substrates.¹² In this study, we demonstrate and characterize electrically injected edge emitting DUV LEDs enabled by MBE grown heterostructures on bulk AlN substrates.

As the core of the LED is a pn junction, there is a need for electron and hole injection layers. For hole injection in ultrawide-bandgap (UWBG) AlGaN, successful use of dopant-free distributed polarization doping (DPD) in high Al content AlGaN pn diodes has been realized in previous studies by both MBE and MOCVD.^{12–14} As shown in Fig. 1(a), for electron injection we design a heterostructure with a heavily silicon doped n⁺-AlGaN region. Combining the polarization and impurity doped layers for p- and n-regions, respectively, we demonstrate a step towards developing a UV-C laser.

We implement a separate confinement heterostructure (SCH) diode with an undoped waveguide layer to confine photons, and a single quantum well to confine electron and hole carriers for recombination. The asymmetric waveguide structure is optimized to have the highest optical mode confinement factor Γ of ~ 6% at 270 nm. We fabricate Fabry-Pérot cavities with cleaved mirror facets. The emitted photons are waveguided in the high refractive index cladding layer and collected from the edge of the cavity.

The LED heterostructure shown in Fig. 1(a) was grown by nitrogen plasma-assisted MBE on a single crystal bulk AlN substrate. The targeted AlGaN epilayers on the metal polar face of the substrate along the [0001] crystal direction are: a 500 nm AlN buffer layer, 400 nm n⁺-Al_{0.76}Ga_{0.24}N with Si donor doping, a 9 nm single quantum well (SQW) sandwiched in a 120 nm asymmetric Al_{0.66}Ga_{0.34}N waveguide layer (50 nm on the n-side and 70 nm on the p-side), a 300 nm unintentionally doped (UID) AlGaN layer linearly

^{a)}Electronic mail: sa2368@cornell.edu

^{b)}Electronic mail: hh494@cornell.edu

^{c)}Electronic mail: djena@cornell.edu

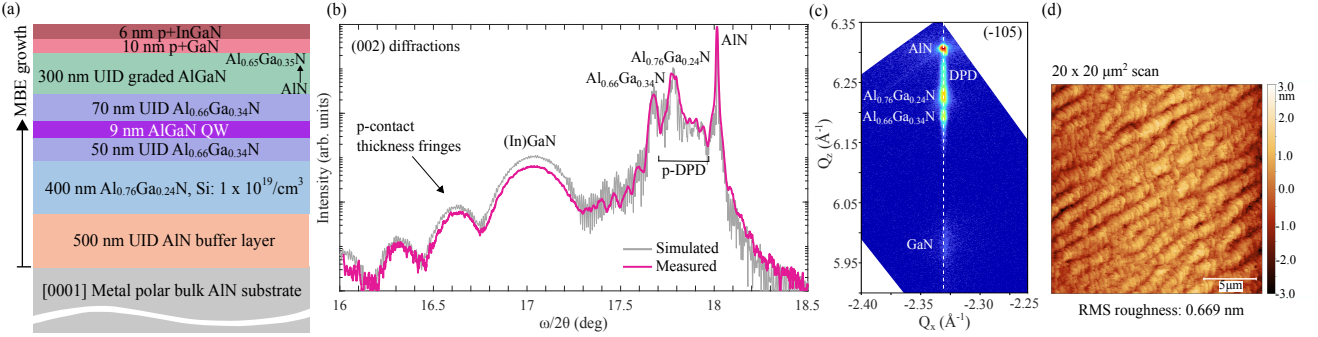
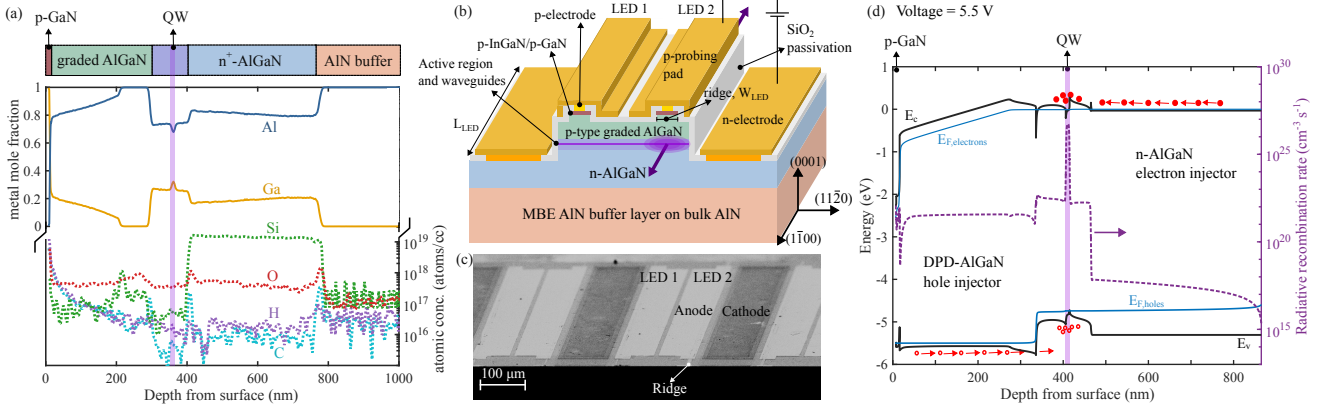


FIG. 1. (a) Heterostructure of the LED used in this study. (b) Measured and simulated symmetric 2θ - ω X-ray diffraction scans across the (002) planes. (c) Reciprocal space map across the asymmetric ($\bar{1}05$) diffractions. (d) $20 \times 20 \mu\text{m}^2$ AFM scan on the surface of the LED.



graded from AlN to Al_{0.65}Ga_{0.35}N along the growth direction resulting in distributed polarization doping creating an effective $\rho_\pi \sim 6 \times 10^{17} \text{ cm}^{-3}$ mobile hole density,¹² and a Mg doped contact layer consisting of 10 nm p⁺GaN and 6 nm p⁺In_{0.05}Ga_{0.95}N.

The targeted Al mole fraction was $\sim 54\%$ in the quantum well for the desired 270 nm wavelength. The symmetric (002) X-ray diffraction scan is shown in Fig. 1(b) along with the theoretical diffraction pattern from a dynamical diffraction model. The extracted AlGaN and InGaN compositions are close to the targeted values. The clearly resolved interference fringes from the thin p-contact layer suggest sharp interfaces throughout the structure and are used to determine the p-contact layer thickness. The asymmetric reciprocal space map of the ($\bar{1}05$) X-ray diffraction scan shown in Fig. 1(c) suggests that all the AlGaN layers are strained to the AlN substrate as desired. Fig. 1(d) shows the atomic force microscopy (AFM) image of the top p-InGaN surface after growth, exhibiting a smooth surface with sub-nanometer surface roughness over $20 \times 20 \mu\text{m}^2$ scan area.

SIMS depth profiles performed at EAG laboratories for Al, Ga, and impurity atoms C, H, Si, and O results are plotted in Fig. 2(a). The Al and Ga metal mole fraction profiles confirm the growth of high Al content Al_xGa_{1-x}N throughout the structure desired for UV-C LEDs and lasers. The relative comparison of the AlGaN composition in the different epilay-

ers is consistent between XRD and SIMS. Expected features like the presence of a quantum well and intentional linear composition grading of the AlGaN distributed polarization doped (DPD) layer are confirmed.

We observe a ~ 70 nm unintentional AlN layer formation at the Al_{0.66}Ga_{0.34}N p-waveguide and the p-DPD interface. Since Al has a strong thermodynamic preference for incorporation over Ga in metal rich MBE growth,¹⁵ the Al/N ratio is varied to control the AlGaN composition. Hence the formation of the AlN interlayer is likely due to an overshoot of the Al metal flux such that $\phi_{\text{Al}}/\phi_{\text{N}} > 1$ causing the growth of binary AlN layer near the interface. Although this UID AlN serves as a desirable electron-blocking layer (EBL), it also is a barrier for hole injection and increases the diode on resistance. The SIMS analysis in the n-AlGaN layer confirms the Si doping level of $\sim 10^{19} \text{ cm}^{-3}$. The C and H levels are at the detection limits throughout the sample. The O level in MBE grown AlN is at the detection limit but is higher in AlGaN layers due to the lower growth temperature of AlGaN than AlN.

Quasi-vertical LEDs were fabricated from the epilayers as shown in Fig. 2(b). Device mesas were formed using chlorine based inductively coupled plasma reactive ion etching (ICP-RIE) ~ 100 nm into the n-AlGaN layer. An additional ridge etch of ~ 200 nm was performed into the DPD layer to define the current aperture. A V/Al/Ni/Au (20/80/40/100 nm)

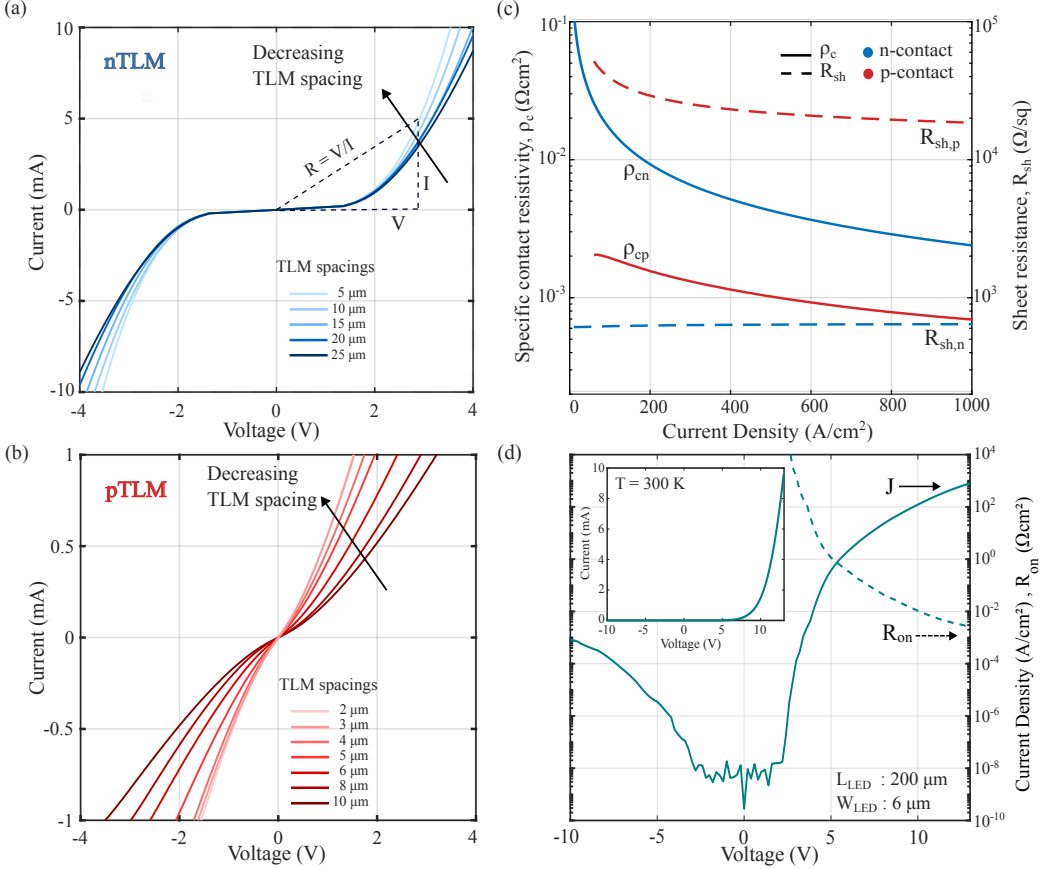


FIG. 3. (a) TLM IVs of the n-contacts. The resistance is calculated at each current value using $R = V/I$ as shown in the figure. (b) TLM IVs of the p-contacts. (c) Specific contact resistivity and sheet resistance of the n- and p-contacts. (d) Linear (inset) and logarithmic diode IV characteristics and specific on resistance (R_{on}) at room temperature.

metal stack was deposited on the etched n-AlGaN surface using electron beam evaporation and annealed at 800°C for 30 s in N₂ ambient. A Ni/Au (15/20 nm) metal stack was deposited on the p-InGaN and annealed at 450°C for 30 s in O₂ ambient and followed by deposition of Ti/Au (20/100 nm) probe pads. SiO₂ was deposited by plasma-enhanced atomic layer deposition (PE-ALD) for 50 nm and then by plasma-enhanced chemical vapor deposition (PECVD) for 200 nm to passivate the device surfaces.

After fabrication into diodes, the AlN substrate was thinned down from $\sim 550 \mu\text{m}$ to $\sim 100 \mu\text{m}$ using mechanical polishing and then cleaved along the (1100) *m*-plane of the crystal into 200 μm to 1000 μm lengths to define Fabry-Pérot cavities. Fig. 2(c) shows the scanning electron microscope (SEM) image of cleaved cavity LED devices with a length $L_{LED} = 200 \mu\text{m}$ and p-electrode widths that range from $W_{LED} = 2\text{-}20 \mu\text{m}$. The anode probing pad, cathode, and the ridge are labeled on the SEM image. The energy band diagram for the LED heterostructure confirmed by SIMS in Fig. 2 (a) is simulated using SiLENSe¹⁶ at 5.5 V forward bias and is shown in Fig. 2(d). Radiative recombination is expected to occur in the QW region by design, as shown by the simulated radiative recombination rates at 5.5 V.

Transfer length method (TLM) pads in rectangular geom-

etry were used to evaluate specific contact resistances of both n- and p-type semiconductor-metal contacts. As shown in Fig. 3(a), the current-voltage (IV) relationship between TLM pairs of n-contact shows barrier-limited transport characteristics and the total resistance shows proportional relationship to TLM pair spacing. To evaluate the non-linear IVs, apparent contact resistance V/I was evaluated at constant current levels for various TLM spacings. The current density is calculated using the effective contact area which is calculated as TLM pad-width $W_{TLM} \times L_t$ (transfer length). Due to the non-linearity of IVs, the specific contact resistivity ρ_c shows dependence on current density J as shown in Fig. 3(c). We acknowledge the uncertainty in the definition of L_t in the case of non-linear contacts. Nonetheless, using a current dependent L_t allows the following rough analysis. The n-contact specific contact resistivity varies from 28 mΩ·cm² at $J \sim 50 \text{ A/cm}^2$ to 4.3 mΩ · cm² at a higher current density of $J \sim 500 \text{ A/cm}^2$. The extracted sheet resistance of n-AlGaN is $\sim 640 \Omega/\square$. From an estimate of mobility $\mu = 30 \text{ cm}^2/\text{V}\cdot\text{s}$, and mobile electron concentration $n = 10^{19} \text{ cm}^{-3}$ assuming full ionization of Si donors, and n-AlGaN layer thickness t after etching = 300 nm, the sheet resistance $R_{sh} = \frac{1}{q \cdot \mu \cdot n \cdot t} \sim 690 \Omega/\square$, which is slightly higher than the R_{sh} value extracted from TLM. This suggests high

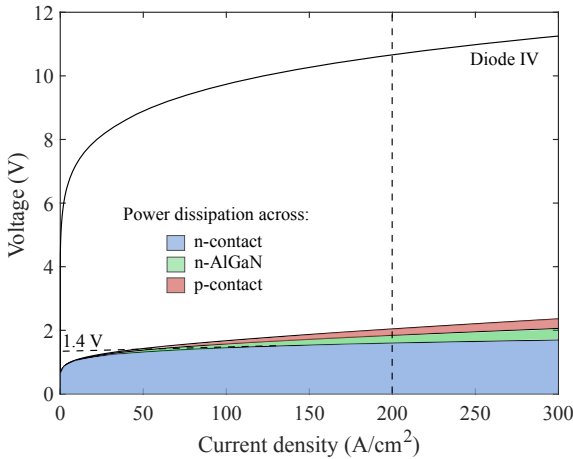


FIG. 4. Voltage drop and power dissipation across different parasitic components as a function of LED current density.

ionization of Si dopants in the n-AlGaN layer and high mobility of electrons. The barrier-limited transport behaviour is likely due to a Schottky barrier and damage caused by the ICP-RIE process and needs to be further studied.

The p-contacts yielded a slightly lower specific contact resistivity of $\sim 2 \text{ m}\Omega\cdot\text{cm}^2$ at low current density of $J \sim 50 \text{ A}/\text{cm}^2$ and $\sim 0.9 \text{ m}\Omega\cdot\text{cm}^2$ at $J \sim 500 \text{ A}/\text{cm}^2$ as shown in Fig. 3(c). The extracted sheet resistance of p-contact layer is $\sim 25 \text{ k}\Omega/\square$. This is similar to the p-contact conductivity determined by Hall-effect measurement prior to fabrication: $6.8 \times 10^{13} \text{ cm}^{-2}$ sheet density, $2.71 \text{ cm}^2/\text{V}\cdot\text{s}$ mobility and $33.9 \text{ k}\Omega/\square$ sheet resistance. The average mobile hole density in the p-contact layers is therefore $6.8 \times 10^{13} \text{ cm}^{-2}/16 \times 10^{-7} \text{ cm} = 4.25 \times 10^{19} \text{ cm}^{-3}$. The high hole concentration and low p-contact resistivity were possible due to the thin InGaN cap layer.¹⁷ Several factors leading to lower specific contact resistivity include: higher activation of Mg dopants in InGaN compared to GaN, favorable 2D hole gas in InGaN induced by polarization charge at the GaN/InGaN heterojunction, and lower Schottky barrier height leading to better tunneling.

The J - V characteristics of the diode at room temperature is shown in Fig. 3(d). An on/off ratio of ~ 5 -6 orders at $\pm 5 \text{ V}$ is observed. The LED turn-on voltage obtained from a linear extrapolation from a current density of $10 \text{ A}/\text{cm}^2$ is $\sim 7.4 \text{ V}$. The high turn-on voltage of the LED is from the non-ohmic metal/semiconductor contacts and is discussed more in the next section. For the quasi-vertical device, we define the diode area as the p-electrode area. We use this area to report the room temperature differential on-resistance of the device evaluated as $R_{\text{on}} \sim 2 \text{ m}\Omega\cdot\text{cm}^2$ at $800 \text{ A}/\text{cm}^2$ and 13 V . Despite the sub-optimal n-contacts, the DUV LEDs were capable of achieving high injection current density on select devices, such as the one shown in Fig. 3 (d).

In Fig. 4 we estimate the voltage drop across different parasitic resistances of the diode shown in Fig. 3(d). The n-contact voltage drop is calculated as $V_{\text{cn}} = \rho_{\text{cn}} \times J_{\text{n}}$, where the specific contact resistivity ρ_{cn} is extracted from the TLM

data shown in Fig. 3, and J_{n} is the current density through the n-electrode. The p-contact voltage drop is calculated using the same method. The lateral resistance of the n-AlGaN layer is evaluated as $V_{\text{lateral}} = I \times R_{\text{n-AlGaN}}$, where I is the current through the diode, and

$$R_{\text{n-AlGaN}} = R_{\text{sh}} \times \frac{d}{L_{\text{LED}}} + R_{\text{sh}} \times \frac{W_{\text{LED}}}{2 \times L_{\text{LED}}},$$

where R_{sh} is the extracted sheet resistance, $d = 17 \mu\text{m}$ is the lateral spacing between the n and p electrodes. The factor of 2 in the second term arises from the assumption that, under low-current conditions, the lateral current distribution decreases linearly from its maximum near the n-electrode mesa to zero at the opposite edge of the p-electrode.

We identify most of the parasitic power to be dissipated across the n-contact, which introduces a turn-on voltage of $\sim 1.4 \text{ V}$ in the diode, as extrapolated from the linear regime of the n-contact IV. This can be mitigated by lowering the n-contact resistance through higher Si doping¹⁸ in n-Al_{0.76}Ga_{0.24}N and improving etching and annealing conditions. As shown in the dashed vertical line in Fig. 4, at a current density of $200 \text{ A}/\text{cm}^2$ and $\sim 10 \text{ V}$ in the diode IV, about $\sim 2 \text{ V}$ is accounted for in the n-contact, 0.21 V from the p-contact and 0.25 V from the n-AlGaN lateral resistance. About $\sim 5 \text{ V}$ is needed for the quasi-Fermi level splitting in the active region, which leaves 2.5 V unaccounted for. The additional series resistance and delayed turn-on voltage may arise from heterojunction barriers (e.g., p-GaN/p-Al_{0.65}GaN_{0.35}, DPD-AlN/UID AlN) and from the UID 70 nm AlN interlayer and waveguides. AlGaN-based DUV LED processing studies have reported that the high temperature n-contact annealing degrades the p-contact.¹⁹⁻²¹ The power dissipation in the n-AlGaN lateral injection resistance can be reduced by minimizing the distance between the n and p-electrodes. While this approach is acceptable for LEDs, placing the p-electrode closer than $\sim 15 \mu\text{m}$ with respect to the mesa edge can increase the threshold current density of a laser diode,²² due to non-radiative recombination at the mesa edge from point defects caused by dry-etching. Increasing the Si doping concentration in the n-AlGaN can help reduce the lateral resistance.

The EL spectrum is collected using an Acton SP2500 monochromator with a 240 nm blazed 2400 g/mm grating. Figure 5(a) shows the EL spectra collected from the cleaved *m*-plane facet of a $200 \mu\text{m} \times 2 \mu\text{m}$ LED operating in CW mode at $T = 273 \text{ K}$ with increasing current density. The highest intensity peak emission wavelength is 265 nm ($\sim 4.7 \text{ eV}$), along with a side peak emission at around 277 nm ($\sim 4.5 \text{ eV}$) occurring at higher current densities. We believe that these 2 peaks are from the UID-Al_{0.66}Ga_{0.34}N waveguide core and the QW layer, respectively, given their peak positions and energy difference. The unwanted recombination in the waveguide layers could be because of electrons that overflow the well and are injected into the p-side of the 70 nm waveguide layer. This was also seen during the development of UV-B laser diodes.²³ Variants of the current heterostructure design with varying waveguide layer thicknesses and compositions will be studied in the future to confirm this hypothesis. No

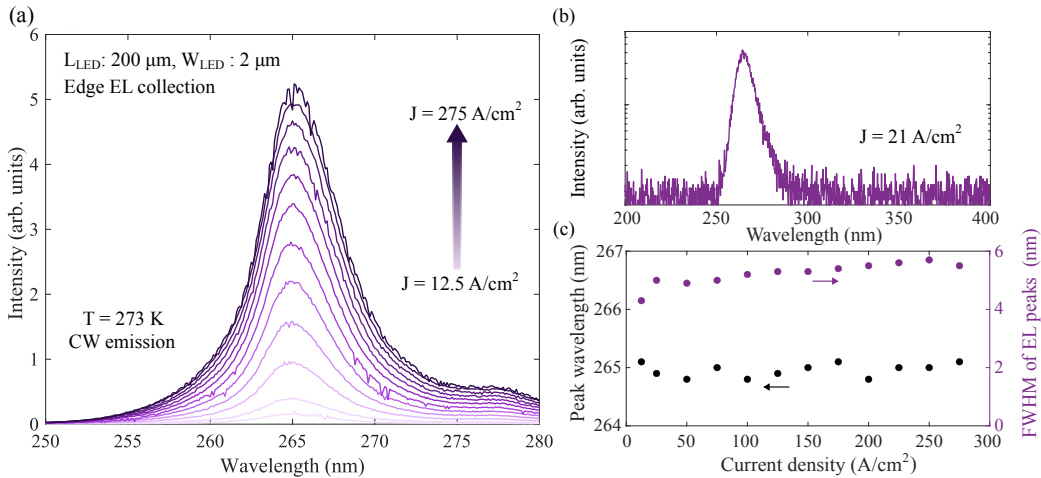


FIG. 5. (a) Current dependent electroluminescence collected from a cleaved edge of the LED. (b) Electroluminescence in logarithmic scale in a wider range from 200-400 nm. (c) Dependence of the peak wavelength and the FWHM of the EL peaks on injection current.

parasitic luminescence is observed till 400 nm as shown in Fig. 5(b). The peak wavelengths do not shift with increasing current up to 275 A/cm². The low full width at half maximum (FWHM) of EL peaks of 5-6 nm indicate composition uniformity in the AlGaN layers. A slight increase of FWHM with current can also be seen due to band filling in Fig. 5(c).

To summarize, we have demonstrated 265 nm UV-C LEDs grown pseudomorphically on bulk AlN substrates by MBE. A high current density up to 800 A/cm² and on/off ratio of 5 orders of magnitude is achieved. We speculate that a high parasitic power dissipation occurs at the n-contact. Therefore, to reduce operating voltages and achieve higher efficiency it is important to lower contact resistances to high composition n-AlGaN. Edge collection of photons was facilitated by a waveguide design and cleaved *m*-plane facets on the devices which are important for the development of UV-C lasers. High energy photons of 4.7 eV energy are collected from the ultrawide bandgap AlGaN active region. This device design and operation is important towards the development of UV-C optoelectronics on the AlN platform.

ACKNOWLEDGMENTS

This work was supported by the Army Research Office under Grant No. W911NF2220177 (characterization); ULTRA, an Energy Frontier Research Center funded by the U.S. Department of Energy (DOE); SUPREME (modeling), one of seven centers in JUMP 2.0, a Semiconductor Research Corporation (SRC) program sponsored by DARPA; and the DARPA UWBGS program. This work was performed in part at the Cornell NanoScale Facility, an NNCI member supported by NSF Grant NNCI 2025233.

AUTHOR DECLARATIONS

S. Agrawal and H.W. Huang contributed equally to this work.

CONFLICT OF INTEREST

The authors have no conflict of interest to declare.

DATA AVAILABILITY STATEMENT

The data that support the findings of this study are available from the corresponding authors upon reasonable request.

- ¹M. Kneissl, T.-Y. Seong, J. Han, and H. Amano, “The emergence and prospects of deep-ultraviolet light-emitting diode technologies,” *Nature Photonics* **13**, 233–244 (2019).
- ²Z. Zhang, A. Yoshikawa, M. Kushimoto, C. Sasaoka, and H. Amano, “Study on degradation of deep-ultraviolet laser diode,” *Physica Status Solidi (a)* **221**, 2300946 (2024).
- ³Z. Zhang, M. Kushimoto, A. Yoshikawa, K. Aoto, C. Sasaoka, L. J. Schowalter, and H. Amano, “Key temperature-dependent characteristics of AlGaN-based UV-C laser diode and demonstration of room-temperature continuous-wave lasing,” *Applied Physics Letters* **121**, 222103 (2022).
- ⁴Y. Cho, C. S. Chang, K. Lee, M. Gong, K. Nomoto, M. Toita, L. J. Schowalter, D. A. Muller, D. Jena, and H. G. Xing, “Molecular beam homoepitaxy on bulk AlN enabled by aluminum-assisted surface cleaning,” *Applied Physics Letters* **116**, 172106 (2020).
- ⁵Y. Chen, C. Haller, W. Liu, S. Y. Karpov, J.-F. Carlin, and N. Grandjean, “GaN buffer growth temperature and efficiency of InGaN/GaN quantum wells: The critical role of nitrogen vacancies at the GaN surface,” *Applied Physics Letters* **118**, 111102 (2021).
- ⁶H. Kobayashi, K. Sato, Y. Okuaki, T. Lee, Y. Kunimi, and N. Kuze, “Enhanced wall-plug efficiency over 2.4% and wavelength dependence of electrical properties at far UV-C light-emitting diodes on single-crystal AlN substrate,” *Physica Status Solidi (RRL)–Rapid Research Letters* **18**, 2400002 (2024).
- ⁷Z. Zhang, J. Encomedero, R. Chaudhuri, Y. Cho, V. Protasenko, K. Nomoto, K. Lee, M. Toita, H. G. Xing, and D. Jena, “Polarization-induced 2D hole gases in pseudomorphic undoped GaN/AlN heterostructures on single-crystal AlN substrates,” *Applied Physics Letters* **119**, 162104 (2021).
- ⁸P. Bagheri, A. Klump, S. Washiyama, M. Hayden Breckenridge, J. H. Kim, Y. Guan, D. Khachariya, C. Quiñones-García, B. Sarkar, S. Rathkanthiwar, *et al.*, “Doping and compensation in heavily Mg doped Al-rich AlGaN films,” *Applied Physics Letters* **120**, 082102 (2022).
- ⁹J. Ruschel, J. Glaab, N. Susilo, S. Hagedorn, S. Walde, E. Ziffer, H. K. Cho, N. L. Ploch, T. Wernicke, M. Weyers, *et al.*, “Reliability of UVC LEDs

fabricated on AlN/sapphire templates with different threading dislocation densities,” *Applied Physics Letters* **117**, 241104 (2020).

¹⁰Z. Ren, Q. Sun, S.-Y. Kwon, J. Han, K. Davitt, Y. Song, A. Nurmikko, W. Liu, J. Smart, and L. Schowalter, “AlGaN deep ultraviolet LEDs on bulk AlN substrates,” *Physica Status Solidi C* **4**, 2482–2485 (2007).

¹¹L. van Deurzen, R. Page, V. Protasenko, K. Nomoto, H. G. Xing, and D. Jena, “Optically pumped deep-UV multimode lasing in AlGaN double heterostructure grown by molecular beam homoepitaxy,” *AIP Advances* **12**, 035023 (2022).

¹²S. Agrawal, L. van Deurzen, J. Encomendero, J. E. Dill, H. Wei Sheena Huang, V. Protasenko, H. G. Xing, and D. Jena, “Ultrawide bandgap semiconductor heterojunction p–n diodes with distributed polarization-doped p-type AlGaN layers on bulk AlN substrates,” *Applied Physics Letters* **124**, 102109 (2024).

¹³M. Ramesh, S. Agrawal, H. G. Xing, and D. Jena, “Ultrawide bandgap channel polarization-doped junction field-effect transistor,” *Physica Status Solidi (a)*, 2401023 (2025).

¹⁴T. Kumabe, A. Yoshikawa, S. Kawasaki, M. Kushimoto, Y. Honda, M. Arai, J. Suda, and H. Amano, “Demonstration of AlGaN-on-AlN pn diodes with dopant-free distributed polarization doping,” *IEEE Transactions on Electron Devices* **71**, 3396–3402 (2024).

¹⁵W. Hoke, A. Torabi, J. Mosca, and T. Kennedy, “Thermodynamic analysis of cation incorporation during molecular beam epitaxy of nitride films using metal-rich growth conditions,” *Journal of Vacuum Science & Technology B: Microelectronics and Nanometer Structures Processing, Measurement, and Phenomena* **25**, 978–982 (2007).

¹⁶“SiLENSe, STR Software for Modeling of Crystal Growth, Epitaxy, and Semiconductor Devices,” .

¹⁷K. Lee, S. Bharadwaj, V. Protasenko, H. Xing, and D. Jena, “Efficient InGaN p-contacts for deep-UV light emitting diodes,” in *2019 Device Research Conference (DRC)* (2019) pp. 171–172.

¹⁸S. Bharadwaj, S. Islam, K. Nomoto, V. Protasenko, A. Chaney, H. G. Xing, and D. Jena, “Bandgap narrowing and Mott transition in Si-doped $\text{Al}_{0.7}\text{Ga}_{0.3}\text{N}$,” *Applied Physics Letters* **114**, 113501 (2019).

¹⁹H.-W. S. Huang, S. Agrawal, D. Bhattacharya, V. Protasenko, H. G. Xing, and D. Jena, “Low p-contact resistance InGaN-capped AlGaN-based DUV LEDs on bulk AlN substrates,” *Applied Physics Letters* **127**, 193305 (2025).

²⁰G.-D. Hao, M. Taniguchi, N. Tamari, and S.-i. Inoue, “Improved turn-on and operating voltages in AlGaN-based deep-ultraviolet light-emitting diodes,” *Journal of Electronic Materials* **46**, 5677–5683 (2017).

²¹D. Bhattacharya, S. Agrawal, H.-W. S. Huang, M. Ramesh, V. Protasenko, H. G. Xing, and D. Jena, “Dielectric-assisted lift-off enabled simultaneous low n- and p-contact resistivities in ultrawide bandgap AlGaN pn diodes on bulk AlN,” (forthcoming in 2026).

²²M. Kushimoto, Z. Zhang, N. Sugiyama, Y. Honda, L. J. Schowalter, C. Sasaoka, and H. Amano, “Impact of heat treatment process on threshold current density in AlGaN-based deep-ultraviolet laser diodes on AlN substrate,” *Applied Physics Express* **14**, 051003 (2021).

²³K. Sato, S. Yasue, Y. Ogino, M. Iwaya, T. Takeuchi, S. Kamiyama, and I. Akasaki, “Analysis of spontaneous subpeak emission from the guide layers of the Ultraviolet-B laser diode structure containing composition-graded p-AlGaN cladding layers,” *Physica Status Solidi (a)* **217**, 1900864 (2020).